Circuits for the Spectroscopic Readout of Bits from Molecular Quantum-dot Cellular Automata

Peizhong Cong, Alexander Rocque, and Enrique P. Blair [a)]
Electrical and Computer Engineering Department, Baylor University, Waco, Texas, USA.

(Dated: 16 September 2024)

Molecular quantum-dot cellular automata (QCA) may provide high speed, low power, classical information processing in the post-CMOS era. The readout of molecular QCA bits is challenging because the molecules may be much smaller than transistors and even single-electron transistors. This paper builds on a recent proposal for the spectroscopic readout of bits from asymmetric QCA molecules. Here, we propose circuits for fanning out a bit onto a large QCA circuit to increase the spectroscopic signal-to-noise ratio. As the number of molecules in a fanout circuit grows, however, the internal bias of each asymmetric cell accumulates, and the circuit may become stuck, tolerating only a very small internal bias. We also propose the use of an applied electric field to compensate for a candidate molecule's internal bias, thereby restoring switchability, even when the internal bias is significant.

I. INTRODUCTION

Quantum-dot cellular automata (QCA)[1] is a paradigm for classical, general-purpose computing designed as a low-power alternative to the transistor. In QCA, the elementary device is a cell, a system of coupled quantum dots with mobile charge. The charge configuration of a cell encodes a bit, and charge tunneling between dots enables device switching. Cells are coupled locally via the electrostatic field, and this interaction allows layouts of cells to function as digital logic circuits.[2] Simpler logic gates may be used to form more complex logic, and even processors have been designed in QCA.[3,4]

Cells have been realized using metallic dots,[5] semiconductor dots,[6] and dangling bonds on a silicon surface.[7] The implementation of interest here is a molecular one, in which redox centers on mixed-valence molecules provide quantum dots.[1,8,9] This may be at the limit of scaling for devices that may be engineered by humanity. Since bit energies are Coulomb energies, and these increase with decreasing distance, molecular QCA may support bit energies robust at ambient temperatures. They may also support device switching at time scales several orders of magnitude shorter than those of commercial CMOS transistors.[10,11]

Molecular QCA candidates have been designed and proposed, and some have been synthesized and studied. Ionic candidate QCA molecules have been attached to a surface and switched.[12,13] Additionally, in recognition that neutralizing charge may locate randomly near ionic QCA cells, changing device characteristics[14–16] and potentially disrupting circuits,[17,18] a class of mixed-valence zwitterionic molecules was proposed, in which neutral species may provide QCA cells.[19,20] A zwitterionic candidate QCA molecule was synthesized and reported in 2015.[21]

Some milestones must be achieved in order to realize the promise of molecular QCA computation. A candidate molecule must be designed, synthesized and tested, and technology must be in place to arrange molecules of this species with adequate precision. Methods for writing classical bits from CMOS to much smaller QCA circuits must be achieved, as well as methods for reading bits from QCA systems.

This paper focuses on a circuit-based approach to support bit readout from QCA circuits. Some proposals for bit readout involves single-electron transistors[22–26] or the use of a single molecules to modify the gating characteristics for a transistor.[27] Our group has recently proposed the use of asymmetric QCA cells for spectroscopic readout of QCA states.[28] This may allow room-temperature readout of QCA bits. We develop this theme by exploring readout circuits comprised of asymmetric QCA cells. The central concept is fanout, the copying of the state of a QCA cell onto many others. For asymmetric readout, the bit should be copied in the same way to each molecule so as to strengthen the spectroscopic signal, increase the signal-to-noise ratio, and provide a larger illumination target for methods such as tip-enhanced Raman spectroscopy (TERS)[29–31] or surface-enhanced Raman spectroscopy (SERS).[32]

Device asymmetry may cause an internal bias toward one device state. This effect grows increasingly significant as the number of cells in a fanout circuit grows. Eventually, the bias may prevent the output circuit from supporting both the "0" and "1" states. We show here that the internal bias may be compensated using an externally-applied electric field.

II. BACKGROUND

A QCA cell is a coupled system of quantum dots with some mobile charge. An example with one mobile electron on a double-quantum-dot (DQD) system is shown in Figure 1. Two localized charge states provide a "0"

[a)]Corresponding author; Electronic mail: Enrique_Blair@baylor.edu

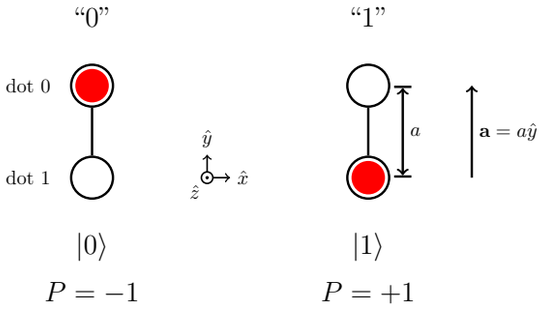

FIG. 1. A mobile electron (red disc) has two localized states on a molecular double-quantum dot system. The dots are represented by circles, and a tunneling path is indicated by a line. The dots are separated by distance a, and the displacement from dot 1 to dot 0 defines a vector $\mathbf{a}$. In this example, $\mathbf{a} = a\hat{y}$.

configuration and a "1" configuration. Layouts of cells may be used to form QCA logic circuits.

The readout of bits from molecular QCA circuits is challenging because even single-electron transistors (SETs) are much larger than QCA molecules, which may have a $\sim 1\,\mathrm{nm}^2$ footprint. Therefore, a spectroscopic readout scheme was proposed recently for molecular QCA. For spectroscopic readout, it is insufficient to have a symmetric molecule. Spectroscopic readout of QCA molecules depends on a dissimilarity between the various charge centers on the molecule, so that different states have distinct Raman spectra. Thus, spectroscopic readout provides a use case for asymmetric QCA molecules.

It is desirable to use many asymmetric molecules, rather than just a single molecule for the spectral readout of QCA bits. The laser spot size will be much larger than the dimensions of a target molecule, and for a single molecule, the signal-to-noise-ratio (SNR) may be very low. Therefore, it will be useful to copy the output bit to many like molecules. This will provide a larger illumination target, as well as enhance the SNR.

One challenge with asymmetric molecules is that they may have an internal bias, Δ_o favoring one state over the other. The effect of this bias becomes more pronounced in a circuit with N asymmetric cells as N grows. This paper describes the effects of Δ_o on circuit behavior and presents spectroscopic readout circuits, in which we compensate for Δ_o by applying an external electric field.

III. MODEL

In this paper, we study circuits comprised of two-dot cells, as shown in Figure 1. The two-dot cell is treated as a two-state system, with localized charge states of a mobile electron providing two classical states, "0" and "1." These states, respectively, are assigned the symbols $|0\rangle$ and $|1\rangle$, as well as polarizations $P = -1$ and $P = +1$. Here, polarization is a function of the mobile charge on the dots: $P = -(q_1 - q_0)/q_e$, where q_k is the mobile charge on dot k, and $-q_e$ is the charge of an electron. Quantum superpositions of the classical states $|0\rangle$ and $|1\rangle$ have values of P intermediate to the extreme values of $P = \pm 1$.

The Hamiltonian for this two-dot cell may be written as

$$\hat{H} = -\gamma\hat{\sigma}_x + \frac{\Delta}{2}\hat{\sigma}_z. \tag{1}$$

Here, the operators $\hat{\sigma}_x = |1\rangle\langle 0| + |0\rangle\langle 1|$ and $\hat{\sigma}_z = |1\rangle\langle 1| - |0\rangle\langle 0|$ are Pauli operators. The tunneling energy, γ, characterizes an electron transfer between the two classical states. The second term describes the bias between the two states:

$$\Delta = \left\langle 1 \middle| \hat{H}_0 \middle| 1 \right\rangle - \left\langle 0 \middle| \hat{H}_0 \middle| 0 \right\rangle, \tag{2}$$

for which $\Delta > 0$ biases the cell toward state "0," and $\Delta < 0$ biases the cell toward state "1." We may further distinguish between different contributions to Δ:

$$\Delta = \Delta_{\text{neigh}} + \Delta_E + \Delta_o\ , \tag{3}$$

where Δ_{neigh} is the bias due to the charge configuration of any neighboring cells; $\Delta_E = -q_e\mathbf{a}\cdot\mathbf{E}$ is the contribution to the bias due to an applied external electric field, $\mathbf{E}$; and, Δ_o is an internal bias due to any dissimilarity between the two dots. The vector $\mathbf{a}$ is a displacement that has magnitude a and a direction that points from dot 1 to dot 0, as shown in Figure 2.

For a given cell, the expectation value of $\hat{\sigma}_z$ defines the cell's polarization: $P = \langle\hat{\sigma}_z\rangle$. The sign of P encodes a bit.

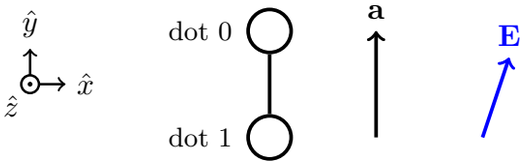

FIG. 2. A double-quantum-dot molecular QCA cell may be immersed in an electric field.

Intercellular Coulomb interactions enable information processing. In Figure 3a, a target cell is placed beside a driver cell and aligned along an axis perpendicular to the $\mathbf{a}$ vector for both cells. We will refer to this as a "row"-type arrangement. In Figure 3b, the target cell is placed at a distance a away from the driver along the $\mathbf{a}$ direction in a "column"-type arrangement. The ground state polarization of the target cell is calculated for both Figures 3a and 3b for various driver polarizations, resulting in cell-cell response curves as shown in Figure 4. For the row configuration, the driver bit is copied with an inversion to the target bit. For the column configuration, a bit is copied from the driver to the target cell. For

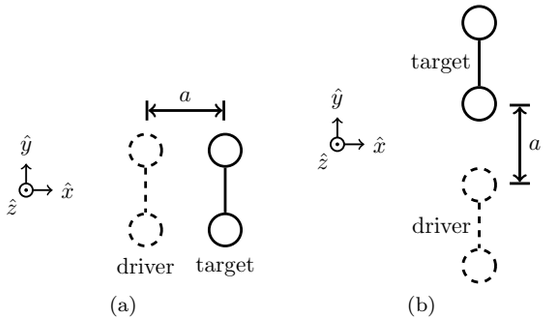

(a) (b)

FIG. 3. A neighboring molecule drives a target molecule. (a) Coupling in the $\pm\hat{x}$ direction is referred to as "row" coupling, and (b) coupling in the $\pm\hat{y}$ direction is called "column" coupling.

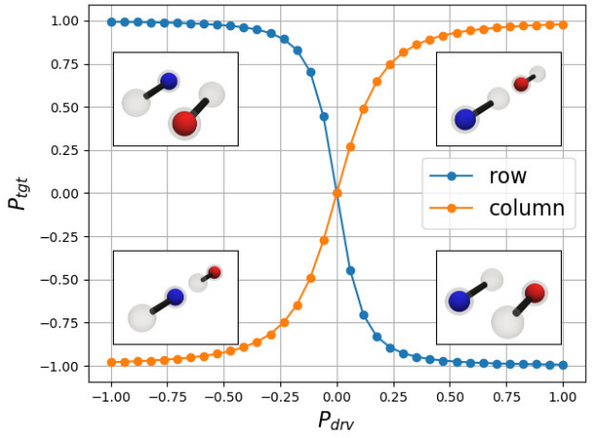

FIG. 4. A driver cell (shown with a blue mobile electron) biases a neighboring molecule (shown with a red mobile electron). (a) When aligned in a row along the $\hat{x}$ direction, the target cell responds by anti-aligning with the driver. (b) When aligned in a column along the $\hat{y}$ direction, the target cell tends to align with the driver cell.

these calculations, $\gamma = 25$ meV was used. In these and all calculations in this paper, $a = 1$ nm is assumed.

To model a QCA circuit, the following general circuit Hamiltonian may be used:

$$\hat{H} = \sum_k \hat{H}_k + \frac{1}{2}\sum_{i,j} E_{i,j}\hat{\sigma}_z^{(i)}\hat{\sigma}_z^{(j)} \,. \tag{4}$$

Here, $\hat{H}_k$ is the free Hamiltonian of cell k. Pair-wise, Coulomb, intercellular coupling is captured in the double summation, where $E_{i,j}$ is an energy of coupling between cells i and j, and the factor of $1/2$ accounts for the double-counting of interactions. $E_{i,j} < 0$ tends to align cells i and j, and $E_{i,j} > 0$ tends to anti-align them. $E_{i,j}$ is determined by the relative positions and orientations of cells i and j.

In this paper, the method for studying a circuit is to calculate the ground state, from which we obtain the polarizations of each cell. We can then take the average of all output polarizations to see whether the circuit as a whole has responded in the desired manner. Circuit inputs are applied using a driver cell, which directly affects only a few cells in the circuit, but may indirectly affect all cells in the fanout circuit.

IV. RESULTS

In this section, it is seen that even a small internal bias in an asymmetric molecule can render a fanout circuit stuck if the number of molecules in the circuit is large enough. This effect is studied, and we explore the use of a compensating electric field to correct circuit behaviors and enable circuit functionality.

A. The Compounding Effects of Internal Bias

Even a small internal bias, Δ_o, can bias an entire circuit strongly so that it is stuck in the preferred state if the number of cells (N) in the circuit is large enough. We explore the effects of the internal bias using fanout circuits of two types, as illustrated in Figures 5a and 5b. The circuit of Figure 5a is straightforward to understand, but the circuit of Figure 5b may provide a higher device density and a higher signal-to-noise ratio under spectroscopic readout.

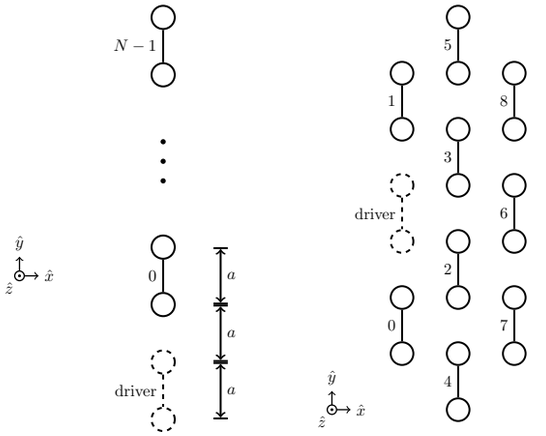

(a) Linear fanout. (b) 2D fanout.

FIG. 5. Circuits used for fanout with asymmetric QCA cells should copy an output bit to multiple cells in the same way. (a) An column array of N cells may function as an output circuit. (b) Fanout also may be accomplished in both the $+\hat{x}$ and $\pm\hat{y}$ directions. This may provide a higher device density and result in a higher spectroscopic SNR.

1. Linear Fanout Circuit

The effects of Δ_o can be understood by considering the linear fanout circuit of Figure 5a. Here, a driver cell simulates a bit resulting from upstream processing and provides a bias for cell 0. The driver bit is then copied onto the column formed by cells 0 through $N-1$. This simple circuit features a design generally desirable in fanout circuits: for low Δ_o, the ground state localizes the charge on each cell in the same manner, contributing to a stronger Raman signal.

For simplicity, we include only nearest-neighbor interactions, so that the circuit Hamiltonian of Equation (4) reduces to

$$\hat{H} = \sum_{k=0}^{N-1} \hat{H}_k + \sum_{j=0}^{N-2} E_{j,j+1} \hat{\sigma}_z^{(j)} \hat{\sigma}_z^{(j+1)} \, . \tag{5}$$

Here, only cell 0 experiences a bias from the driver, so that the Hamiltonian for cell 0 is

$$\hat{H}_0 = -\gamma \hat{\sigma}_x^{(0)} + \left(\frac{\Delta_{drv} + \Delta_o + \Delta_E}{2} \right) \hat{\sigma}_z^{(0)} \, , \tag{6}$$

where $\Delta_{\text{neigh}} = \Delta_{drv}$ is the bias on cell 0 due to the charge configuration of the driver. The Hamiltonian for cells having $k > 0$ may be written as

$$\hat{H}_k = -\gamma \hat{\sigma}_x^{(k)} + \frac{\Delta_o + \Delta_E}{2} \hat{\sigma}_z^{(k)} \, , \tag{7}$$

where only the internal bias Δ_o and the bias Δ_E due to the applied external field $\mathbf{E}$ are included. It can be shown that for cells in this column with a fixed neutralizing charge of $+q_e/2$ on each dot, the nearest-neighbor, pairwise interaction energy is

$$E_{j,j+1} = -\frac{q_e^2}{24\pi\varepsilon_0 a}, \tag{8}$$

where ε_0 is the permittivity of free space. When $a = 1$ nm, $E_{j,j+1} = -240$ meV.

Imposing the restrictions $\gamma = 0$ and $\mathbf{E} = 0$ (no applied field) further simplifies the problem so that $\hat{H}$ is diagonal and most easily analyzed. Consider a state $\vec{x} = b_{N-1} \cdots b_1 b_0$, where $b_k \in \{0, 1\}$ is a classical state of the k-th cell. Each cell in state "0" ($b_k = 0$) contributes $-\Delta_o/2$ to the total energy for being in the internally-biased state, or $\Delta_o/2$ for being in state "1" ($b_k = 1$). Each anti-aligned nearest-neighbor pair $(j, j+1)$ contributes $E_{j,j+1}/2$, and each aligned nearest-neighbor pair contributes $-E_{j,j+1}/2$. Cell 0 contributes $-\Delta_{drv}/2$ when aligned with the driver, and $\Delta_{drv}/2$ when anti-aligned with the driver.

For the readout application, we are most interested in having all cells in state "0" or all in state "1," corresponding to circuit states $|\vec{0}\rangle = |00\cdots0\rangle$ and $|\vec{1}\rangle = |11\cdots1\rangle$. Since these states have $N-1$ nearest-neighbor pairs, we write their energies as

$$E_{\vec{0}} = -\frac{\Delta_{drv}}{2} - N\frac{\Delta_o}{2} + (N-1)\frac{E_{j,j+1}}{2}, \text{ and} \tag{9}$$

$$E_{\vec{1}} = \frac{\Delta_{drv}}{2} + N\frac{\Delta_o}{2} + (N-1)\frac{E_{j,j+1}}{2}. \tag{10}$$

If $\Delta_{drv} > 0$ and $\Delta_o > 0$, then the circuit is biased toward the state $\vec{0}$. On the other hand, when $\Delta_{drv} < 0$ and $\Delta_o > 0$, the driver biases cell 0 toward the state "1" in opposition to the internal bias, which biases all cells toward state "0". In this case, the circuit can bear state "1" as the desired output state only if $E_{\vec{1}} < E_{\vec{0}}$. Thus, we require $\Delta_{drv} < -N\Delta_o$, which provides a constraint on the size of Δ_o:

$$\Delta_o < -\frac{\Delta_{\max}}{N} \tag{11}$$

for some maximum driver bias, $\Delta_{\max}$. Thus, as the circuit size N increases, the output circuit requires molecules with smaller internal biases in order to allow both states $|\vec{0}\rangle$ and $|\vec{1}\rangle$ to be possible as output states. When this condition is not met, state $\vec{1}$ never will be accessible for $\Delta_o > 0$.

As an application of this, we assume an internal bias of $\Delta_o = 50$ meV for all cells, and determine how large N may be in the column of Figure 5a before the circuit fails to a stuck state. The maximum driver bias is equivalent to the pair-wise interaction energy: $\Delta_{\max} = E_{j,j+1} = -240$ meV, the maximum possible driver bias toward "1" on the driver cell. Then, we can use Equation (11) to determine the maximum N for which the driver (cell 0) can drive a successful fanout to either $|\vec{0}\rangle$ or $|\vec{1}\rangle$:

$$N < -\frac{\Delta_{\max}}{\Delta_o} \, . \tag{12}$$

The values used here require $N < 4.8$, consistent with the simulation results shown in Figure 6. The insets with a blue frame correspond to the blue data points, with $P_{drv} = -1$; and, the orange insets illustrate the case for $P_{drv=1}$. Here, $P_{drv} = -1$ (input state "0") drives an average polarization on all the target cells of $\bar{P} = -1$ in all cases, since both Δ_o and P_{drv} bias the system toward $|\vec{0}\rangle$. On the other hand, when $P_{drv} = 1$ in opposition to $\Delta_o > 0$, the accumulating effect of Δ_o with increasing N overwhelms $P_{drv} = 1$, and the fanout of the input bit "1" fails for $N \geq 5$: the average polarization fails to $\bar{P} = -1$. We use as our figure of merit the average polarization, $\bar{P}$, since we are interested in the spectroscopic response of the entire circuit:

$$\bar{P} = \frac{1}{N} \sum_{k=0}^{N-1} P_k \, , \tag{13}$$

where P_k is the polarization of the k-th cell.

We now explore how large $|\Delta_o|$ may be before the circuit fails, given $N = 9$. The plot of Figure 7 shows the average polarization, $\bar{P}$, of all cells in the fanout circuit

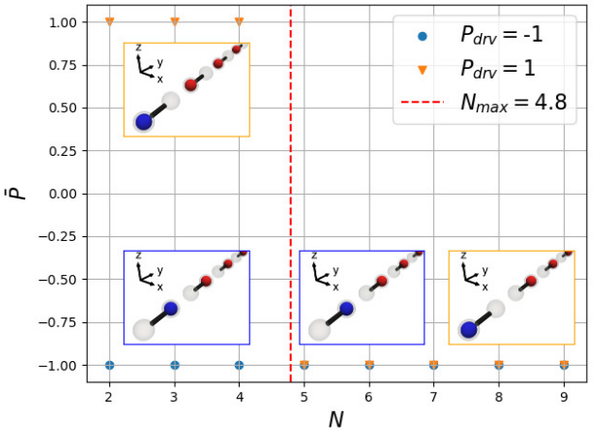

FIG. 6. A fanout column of N asymmetric QCA cells with an internal bias Δ_o fails as N grows too large. Here, the maximum bias from the driver is the same as the coupling energy, $\Delta_{\max} = E_{j,j+1} = -240$ meV. For cells of length $a = 1$ nm and an internal bias of $\Delta_o = 50$ meV, the fanout circuit fails to respond to an input "1" bit with an output state "$11\cdots1$" (desired average polarization of 1) when N exceeds 4, since for $N \geq 5$, the constraint of Equation (11) is not satisfied.

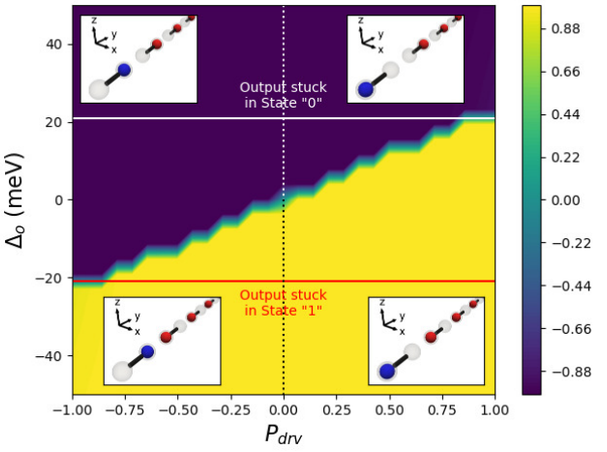

FIG. 7. For a simple fanout onto a line of $N = 9$ cells using longitudinal coupling, a sufficiently large internal bias, $\Delta_o \sim 22$ meV, renders the circuit unable to switch between both outputs. This calculation was performed with $a = 1$ nm and $\gamma = 20$ meV.

as a function of driver polarization, P_{drv}, and internal bias, Δ_o. Here, there is no applied field, $\mathbf{E} = 0$. Ideally, any $P_{drv} > 0$ would lead to an average polarization $\bar{P} \simeq 1$. Similarly, any $P_{drv} < 0$ would lead to an average polarization $\bar{P} \simeq 1$. Thus, the right hand of Figure 7 ($P_{drv} > 0$) ideally would be yellow, and the left hand ($P_{drv} < 0$) would be blue. In this case, however, the increasing Δ_o above zero makes it more difficult to obtain an output circuit state of $|\vec{1}\rangle$. Eventually, $|\vec{1}\rangle$ becomes inaccessible using cell 0 as the sole input bias to the circuit for $\Delta_o \gtrsim 22$ meV. Similarly, the state $|\vec{0}\rangle$ is inaccessible for $\Delta_o \lesssim -22$ meV. Thus, we identify $|\Delta_o|_{\max} = 22$ meV as the maximum allowable $|\Delta_o|$ before the circuit is completely stuck in one state. The insets of Figure 7 show the driver with a blue mobile electron, and a few of the closest cells to the driver are shown with a red mobile electron. The upper right and lower left insets show the fanout array unresponsive to the driver because $|\Delta_o|$ is too large for the nine-cell fanout. $N = 9$ is a very small fanout circuit, but because of Equation (12), a much larger and more reasonable N would restrict the molecules to a much smaller maximum internal bias, $|\Delta_o|_{\max}$.

Decreasing γ increases electron confinement and sharpens the cell-cell polarization response. Conversely, increasing γ weakens the polarization response of QCA cells, and thus the $\bar{P}$ response is degraded, with a much smoother transition between $\bar{P} \sim +1$ regions and $\bar{P} \sim -1$ regions. Figure 8 shows the output circuit response $\bar{P}$ calculated for $\gamma \in \{10, 50, 100\}$ meV. These results are summarized in Table I. For this type of QCA output molecule, low γ is desirable.

TABLE I. For a fanout column consisting of $N = 9$ cells, increasing the the tunneling energy degrades the circuit response by reducing electronic confinement. This reduces the maximum allowable bias, $|\Delta_o|_{\max}$.

γ (meV)	$\lvert\Delta_o\rvert_{\max}$ (meV)
10	25
25	22
50	21
100	13

2. A 2D Fanout Circuit

Similar effects of Δ_o also are seen in the more complex fanout circuit of Figure 5b. Again, the circuit is designed to copy the driver bit onto all cells in the circuit. This provides a higher device density than does the circuit of Figure 5a, and so may provide a higher SNR under spectroscopic readout. While the circuit considered here has only 9 cells for computational tractability, this circuit could be extended in the $+\hat{x}$ and $\pm\hat{y}$ directions for a much larger multiplicity of bit copies and a stronger SNR. In modeling this circuit, we include all pairwise interactions, $E_{i,j}$. Along with the consideration here of $\gamma \neq 0$, this gives rise to a more complex response.

The ground state of the 2D fanout circuit from Figure 5b in response to the driver polarization was calculated for various values of Δ_o, zero applied field, $\mathbf{E} = 0$, $\gamma = 10$ meV, and with $N = 9$ cells. The circuit response, $\bar{P}$, is plotted in the color map of Figure 9. The output circuit's response $\bar{P}$ degrades as $|\Delta_o|$ increases, and eventually becomes stuck for $|\Delta_o| \gtrsim 25$ meV ($|\Delta_o|_{\max} \simeq 25$ meV). Much larger circuits are intractable using the model presented here because of the exponen-

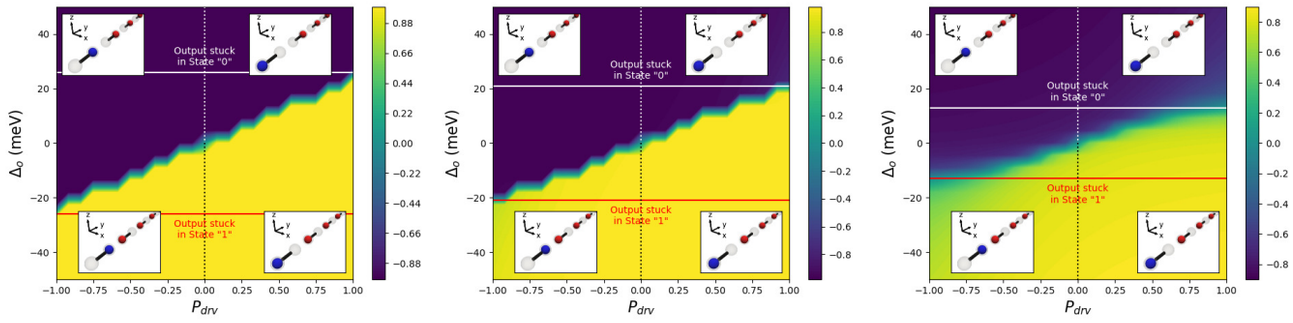

(a) $\gamma = 10$ meV; $|\Delta_o|_{\max} \simeq 25$ meV. (b) $\gamma = 50$ meV; $|\Delta_o|_{\max} \simeq 21$ meV. (c) $\gamma = 100$ meV; $|\Delta_o|_{\max} \simeq 13$ meV.

FIG. 8. Increasing the tunneling energy γ degrades the circuit response by decreasing electronic localization and decreasing cell polarization. As a result, the $\bar{P}$ response becomes smoother with increasing γ. This also decreases the maximum bias strength $|\Delta_o|_{\max}$ allowable before the the circuit becomes stuck decreases. Calculations were peformed for (a) $\gamma = 10$ meV; (b) $\gamma = 50$ meV; and (c) $\gamma = 100$ meV.

tial growth of the circuit's state space with growing circuit size, N; still, we expect that as N increases, the circuit will be have a decreasing $|\Delta_o|_{\max}$.

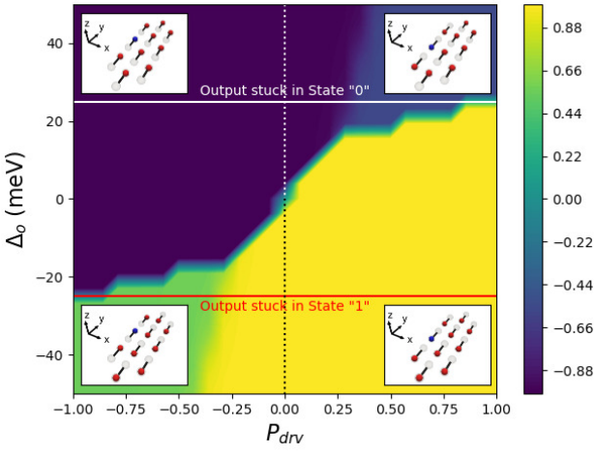

FIG. 9. The internal bias Δ_o also may cause more complex fanout circuits to become stuck. For a fanout circuit comprised of $N = 9$ cells, the output circuit becomes stuck as $|\Delta_o|$ approaches 26 meV. For a much larger fanout on a much larger circuit, only a very small $|\Delta_o|$ will be tolerable before the circuit is stuck (i.e., Δ_o overwhelms the driving bias Δ).

To demonstrate that increasing (reducing) the number of cells N in the circuit reduces (increases) the maximum allowable internal bias, $|\Delta_o|_{\max}$, we remove one and two cells from the circuit of Figure 5b. The removal of two cells results in the circuit of Figure 5b results in the circuit of Figure 10a, and the removal of one cell results in the circuit of Figure 10b.

A calculation of $\bar{P}$ for the circuits of Figures 10a and 10b is shown in Figure 11a. Here, the maximum bias strength before the circuit is stuck is $|\Delta_o|_{\max} \simeq 60$ meV. With one more cell $|\Delta_o|_{\max}$ is reduced to about 38 meV,

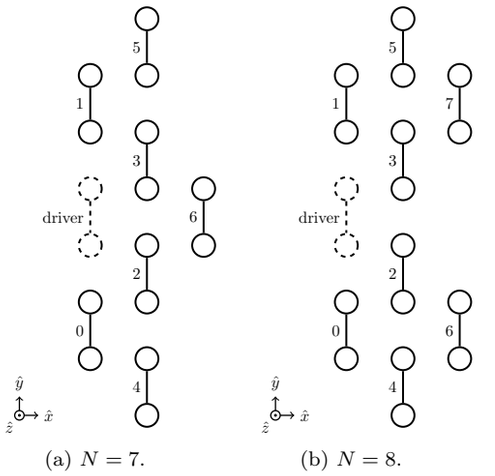

(a) $N = 7$. (b) $N = 8$.

FIG. 10. Cells are removed from the fanout circuit of Figure 5b. (a) Two cells are removed, resulting in a fanout with $N = 7$. (b) One cell is removed, resulting in a fanout with $N = 8$.

TABLE II. For a 2D fanout circuit, increasing the number of cells decreases the maximum allowable bias, $|\Delta_o|_{\max}$

Cells in 2D fanout	$\lvert\Delta_o\rvert_{\max}$ (meV)
7	60
8	38
9	22

as seen in Figure 11b. These results also are summarized in Table II.

A practical fanout circuit may have an N several orders of magnitude greater than those modeled here. In this case, a circuit with large N will likely tolerate negligible internal biases. However, we propose the use of an applied electric field to compensate for the internal bias

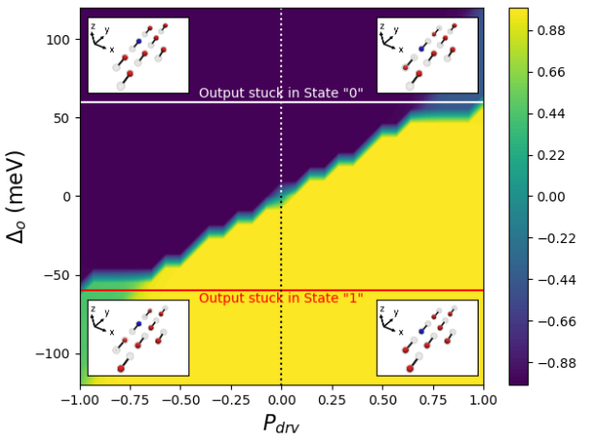

(a) $N = 7$ and $|\Delta_o|_{\max} \simeq 60$ meV.

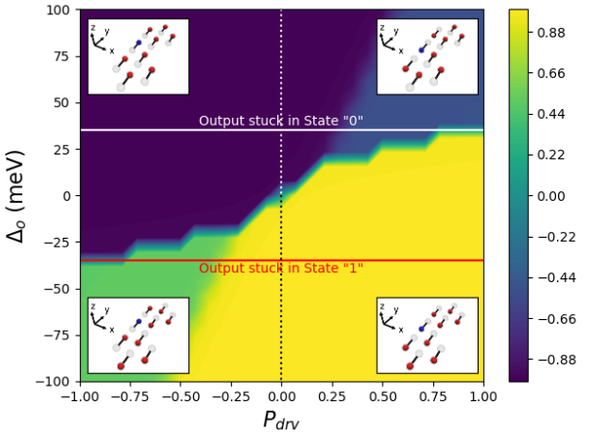

(b) $N = 8$ and $|\Delta_o|_{\max} \simeq 38$ meV.

FIG. 11. Increasing (decreasing) the number of cells, N, in the fanout, decreases (increases) the allowable bias, $|\Delta_o|_{\max}$, before the circuit is completely stuck and cannot output both states $|\vec{0}\rangle$ and $|\vec{1}\rangle$. Compare these values of $|\Delta_o|_{\max}$ with the $|\Delta_o|_{\max} \simeq 25$ meV for the $N = 9$ case.

of an asymmetric QCA molecular species. This is the focus of the next section of the results.

B. Field-Compensated Output Circuits

An applied electric field may be used to compensate for the internal bias in a molecular species used for fanout circuits in a spectroscopic readout application. For a given internal bias, Δ_o, a compensating field component is $E_y\hat{y}$, with E_y given by

$$E_y = -q_e \frac{\Delta_o}{a} \,. \tag{14}$$

This compensating field may be applied using electrodes as illustrated in Figure 12. A voltage, v_c, is applied to the electrodes, which establishes the field with

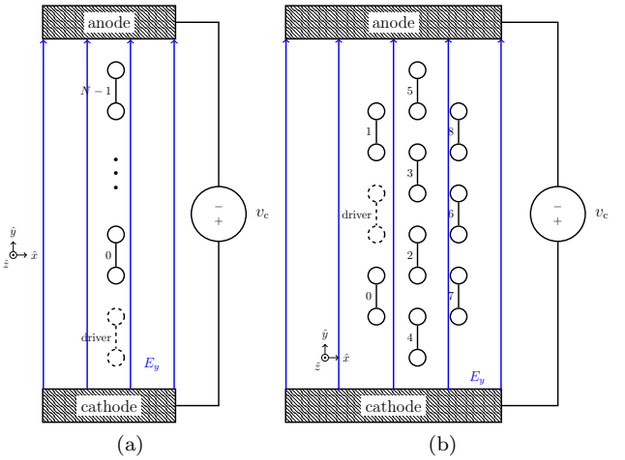

FIG. 12. Electrodes may be used to apply a compensating electric field component, $E_y\hat{y}$, to cancel the effects of the internal bias Δ_o in each molecule.

a bias-compensating component, $E_y\hat{y}$. This is illustrated for the linear fanout circuit in Figure 12a, and again for the 2D fanout circuit in Figure 12b.

To model the compensated circuits of Figure 12, we applied the compensating field from Equation (14) uniformly to all cells. The ground state was calculated for various Δ_o and P_{drv}, yielding the $\bar{P}$ shown in the color map of Figure 13 in the case of the linear fanout with nearest-neighbor interactions only. Notably, the result is the ideal response plot, where $P_{drv} > 0$ results in $\bar{P} \simeq 1$, and $P_{drv} < 0$ results in $\bar{P} \simeq -1$. A similar result for the field-compensated 2D fanout circuit is shown in Figure 14.

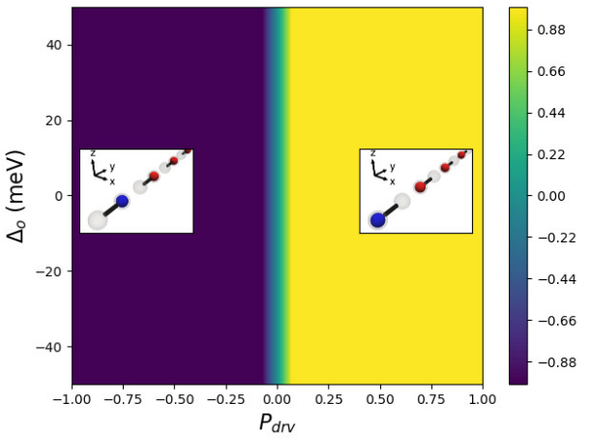

FIG. 13. An applied electric field corrects for the internal bias in a linear fanout circuit for various values of the internal bias, Δ_o.

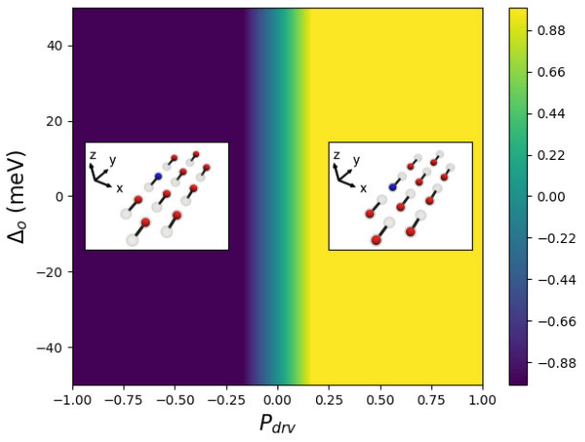

FIG. 14. An applied electric field compensates for the internal bias in a 2D fanout circuit for various values of the internal bias, Δ_o.

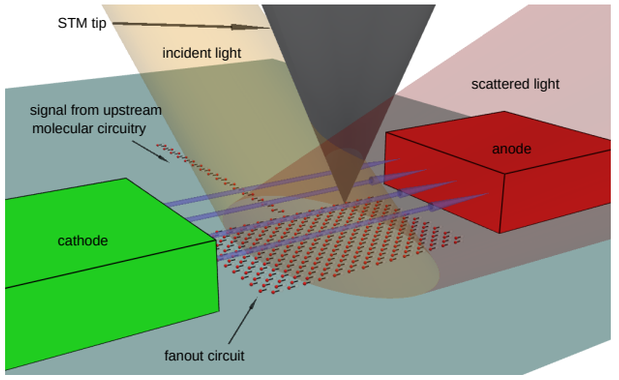

FIG. 15. The proposed readout circuit involves the fanout of a bit onto a circuit of asymmetric molecules. Here, a TERS readout method is illustrated, and charged electrodes provide the bias-compensating field with a direction indicated using the blue arrows. Note: the elements of this illustration are not drawn to scale.

V. DISCUSSION

The electric-field compensation for the effects of the molecular internal bias Δ_o in readout circuits recalls the use of electrodes for input circuits we previously proposed.[33,34] Fringing fields from input electrodes may be tolerated by QCA computational circuitry,[35] suggesting that QCA logic may also function in the presence of charged output electrodes.

This method depends on the ability to effectively cancel the internal bias, Δ_o. This assumes the ability to layout circuits with adequate precision in terms of position and rotation. This study was done using the ground state and does not account for finite temperature. It is likely that thermal effects and entropy may degrade fanout circuit operation;[36] on the other hand, the asymmetric readout circuits proposed here may be extensible to clocked molecular QCA.[37–41] Clocking may mitigate thermodynamic effects and improve order in fanout circuits at room temperature. We have focused on two-dot cells to keep the circuit state space manageable and calculations tractable.

VI. CONCLUSION

We have proposed a circuit-based method for enhancing the SNR in spectroscopic readout of molecular QCA. Illustrated in Figure 15 (not drawn to scale), this involves the fanout of an output bit onto manifold copies on a circuit comprised of asymmetric QCA cells. The internal bias due to molecular asymmetry may be disruptive to circuit operation, making one output state of the circuit inaccessible and leaving the circuit stuck in the other output state. Calculations of the circuit ground state show that we may compensate for the internal molecular bias using an applied electric field. We have also proposed the use of charged electrodes to generate the desired field. Figure 15 shows two-dot cells for consistency with this paper, but three-dot-cells may be desirable to support clocking and its attendant benefits. This output scheme remains compatible with electric-field clocking[40,41] and electric-field inputs,[33,42] since the z-component of the field may be used for clocking, but the bias compensation in this paper uses the y component. While input and output circuits may both use the y component of their respective local fields, spatial separation between inputs and outputs may prevent unwanted interference.

ACKNOWLEDGMENTS

This work was funded in part by the Office of Naval Research under grant N00014-20-1-2420.

DATA AVAILABILITY STATEMENT

The data that support the findings of this study are available from the corresponding author upon reasonable request.

[1] C. S. Lent, "Molecular electronics - bypassing the transistor paradigm," Science **288**, 1597–1599 (2000).
[2] P. Tougaw and C. Lent, "Logical devices implemented using quantum cellular automata," J. Appl. Phys. **75**, 1818–1825 (1994).
[3] M. Niemier, M. Kontz, and P. Kogge, "A design of and design tools for a novel quantum dot based microprocessor," in Proc. of the 37th Design Automation Conf. (2000) pp. 227–232.
[4] K. Walus, M. Mazur, G. Schulhof, and G. Jullien, "Simple 4-bit processor based on quantum-dot cellular automata (qca)," in 2005 IEEE International Conference on Application-Specific Systems, Archite (IEEE, 2005) pp. 288–293.
[5] G. L. Snider, O. Orlov, I. Amlani, G. H. Bernstein, C. S. Lent, J. L. Merz, and W. Porod, "A functional cell for quantum-dot cellular automata," Solid-state Electronics **42**, 1355–1359 (1998).

[6]C. Smith, S. Gardelis, A. Rushforth, R. Crook, J. Cooper, D. Ritchie, E. Linfield, Y. Jin, and M. Pepper, "Realization of quantum-dot cellular automata using semiconductor quantum dots," SUPERLATTICES AND MICROSTRUCTURES **34**, 195–203 (2003), 6th International Conference on New Phenomena in Mesoscopic Structures/4th International Conference on Surfaces and Interfaces of Mesoscopic Devices, Maui, HI, DEC 01-05, 2003.

[7]M. B. Haider, J. L. Pitters, G. A. DiLabio, L. Livadaru, J. Y. Mutus, and R. A. Wolkow, "Controlled coupling and occupation of silicon atomic quantum dots at room temperature," Phys. Rev. Lett. **102**, 046805 (2009).

[8]M. Lieberman, S. Chellamma, B. Varughese, Y. Wang, C. Lent, G. Bernstein, G. Snider, and F. Peiris, "Quantum-dot cellular automata at a molecular scale," Ann. N.Y. Acad. Sci. **960**, 225–239 (2002).

[9]C. Lent, B. Isaksen, and M. Lieberman, "Molecular quantum-dot cellular automata," J. Am. Chem. Soc. **125**, 1056–1063 (2003).

[10]P. Tougaw and C. Lent, "Dynamic behavior of quantum cellular automata," J. Appl. Phys. **80**, 4722 (1996).

[11]E. Blair, S. Corcelli, and C. Lent, "Electric-field-driven electron-transfer in mixed-valence molecules," J Chem Phys **145**, 014307 (2016).

[12]Z. Li, A. M. Beatty, and T. P. Fehlner, "Molecular qca cells. 1. structure and functionalization of an unsymmetrical dinuclear mixed-valence complex for surface binding," Inorganic Chemistry **42**, 5707–5714 (2003), pMID: 12950221, https://doi.org/10.1021/ic026254y.

[13]H. Qi, S. Sharma, Z. Li, G. Snider, A. Orlov, C. Lent, and T. Fehlner, "Molecular quantum cellular automata cells. electric field driven switching of a silicon surface bound array of vertically oriented two-dot molecular quantum cellular automata," J. Am. Chem. Soc. **125**, 15250–15259 (2003).

[14]M. Manimaran, G. Snider, C. Lent, V. Sarveswaran, M. Lieberman, Z. Li, and T. Fehlner, "Scanning tunneling microscopy and spectroscopy investigations of qca molecules," Ultramicroscopy **97**, 55–63 (2003).

[15]H. Qi, A. Gupta, B. Noll, G. Snider, Y. Lu, C. Lent, and T. Fehlner, "Dependence of field switched ordered arrays of dinuclear mixed-valence complexes on the distance between the redox centers and the size of the counterions," J. Am. Chem. Soc. **127**, 15218–15227 (2005).

[16]N. Liza, D. J. Coe, Y. Lu, and E. P. Blair, "Ab initio studies of counterion effects in molecular quantum-dot cellular automata," Journal of Computational Chemistry **45**, 392–404 (2024), https://onlinelibrary.wiley.com/doi/pdf/10.1002/jcc.27247.

[17]P. Tougaw and C. Lent, "Effect of stray charge on quantum cellular automata," Jpn. J. Appl. Phys. **34**, 4373–4375 (1995).

[18]M. LaRue, D. Tougaw, and J. Will, "Stray charge in quantum-dot cellular automata: A validation of the intercellular hartree approximation." IEEE T. Nanotechnol. **12**, 225–233 (2013).

[19]Y. Lu and C. Lent, "Self-doping of molecular quantum-dot cellular automata: mixed valence zwitterions," Phys. Chem. Chem. Phys. **13**, 14928–14936 (2011).

[20]Y. Lu and C. Lent, "Counterion-free molecular quantum-dot cellular automata using mixed valence zwitterions: A double-dot derivative of the [closo-1-cb9h10] cluster," Chem. Phys. Lett. **582**, 86–89 (2013).

[21]J. Christie, R. Forrest, S. Corcelli, N. Wasio, R. Quardokus, R. Brown, S. Kandel, Y. Lu, C. Lent, and K. Henderson, "Synthesis of a neutral mixed-valence diferrocenyl carborane for molecular quantum-dot cellular automata applications," Angewandte Chemie **127**, 15668–15671 (2015).

[22]X. Luo, A. Orlov, and G. Snider, "Origin of coulomb blockade oscillations in single-electron transistors fabricated with granulated cr/cr2o3 resistive microstrips," Microelectr. J. **36**, 308–312 (2005).

[23]H. Brenning, S. Kafanov, T. Duty, S. Kubatkin, and P. Delsing, "An ultrasensitive radio-frequency single-electron transistor working up to 4.2k," J. Appl. Phys. **100**, 114321 (2006).

[24]A. Prager, A. Orlov, and G. Snider, "Integration of cmos, single electron transistors, and quantumdot cellular automata," in Proc. of the 2009 IEEE Nanotechnolog Materials and Devices Conference (NM (2009).

[25]R. Joyce, H. Qi, T. Fehlner, C. Lent, A. Orlov, and G. Snider, "A system to demonstrate the bistability in molecules for application in a molecular qca cell," in IEEE Nanotechnology Materials and Devices Conference (IEEE, 2009).

[26]Y. Lee, V. Joshi, A. Orlov, and G. Snider, "Si single electron transistor fabricated by chemical mechanical polishing," J. Vac. Sci. Technol. B **28** (2009).

[27]A. Pulimeno, M. Graziano, D. Demarchi, and G. Piccinini, "Towards a molecular qca wire: Simulation of write-in and read-out systems," Solid State Electron. **77** (2012).

[28]N. Liza, D. Murphey, P. Cong, D. Beggs, Y. Lu, and E. Blair, "Asymmetric, mixed-valence molecules for spectroscopic readout of quantum-dot cellular automata," Nanotechnology **33**, 115201 (2022).

[29]N. Hayazawa, Y. Inouye, Z. Sekkat, and S. Kawata, "Metallized tip amplification of near-field raman scattering," Optics Commun. **183**, 333–336 (2000).

[30]R. Stöckle, Y. Suh, V. Deckert, and R. Zenobi, "Nanoscale chemical analysis by tip-enhanced raman spectroscopy," Chem. Phys. Lett. **318**, 131–136 (2000).

[31]M. Anderson, "Locally enhanced raman spectroscopy with an atomic force microscope," Appl. Phys. Lett. **76**, 3130 (2000).

[32]B. Pettinger, G. Picardi, R. Schuster, and G. Ertl, "Surface enhanced raman spectroscopy: Towards single molecule spectroscopy," Electrochemistry **68**, 942 (2000).

[33]E. Blair, "Electric-field inputs for molecular quantum-dot cellular automata circuits," IEEE T. Nanotechnol. **18**, 453–460 (2019).

[34]P. Cong and E. Blair, "arxiv:2103.03396 [quant-ph],".

[35]P. Cong and E. Blair, "Clocked molecular quantum-dot cellular automata circuits tolerate unwanted external electric fields," J. Appl. Phys **131** (2022).

[36]C. Lent, P. Tougaw, and W. Porod, "Quantum cellular automata: the physics of computing with arrays of quantum dot molecules," in Workshop on Physics and Computation, PHYSCOMP'94 Proceedings (1994) pp. 5–13.

[37]G. Bernstein, G. Bazan, M. Chen, C. Lent, J. Merz, A. Orlov, W. Porod, G. Snider, and P. Tougaw, "Practical issues in the realization of quantum-dot cellular automata," Superlattice. Microst. , 447–459 (1996).

[38]G. Tóth and C. Lent, "Quasi-adiabatic switching for metal-island quantum-dot cellular automata," J. Appl. Phys. **85**, 2977–2984 (1999).

[39]J. Timler and C. Lent, "Maxwell's demon and quantum-dot cellular automata," J. Appl. Phys. **94**, 1050–1060 (2003).

[40]K. Hennessy and C. S. Lent, "Clocking of molecular quantum-dot cellular automata," Journal of Vacuum Science & Technology B **19**, 1752–1755 (2001).

[41]E. Blair and C. Lent, "An architecture for molecular computing using quantum-dot cellular automata," in IEEE C Nanotechnol., Vol. 1 (IEEE, 2003) pp. 402–405.

[42]P. Cong and E. Blair, "Robust electric-field input circuits for clocked molecular quantum-dot cellular automata," Nanotechnology **21**, 424–433 (2022).